


Nonlinear dynamics in an optoelectronic feedback delay oscillator with piecewise linear transfer functions from the laser diode and photodiode

Géraud R. Goune Chengui^{1,*}, Kengne Jacques,¹ Paul Wofo,² and Yanne K. Chembo³

¹Laboratoires d'Automatique et Informatique Appliquée (UR-AIA), Department of Electrical Engineering, IUT-FV Bandjoun, P.O. Box 134, Bandjoun, Cameroon

²Laboratory of Modelling and Simulation in Engineering, Biomimetics and Prototypes, Department of Physics, Faculty of Science, P.O. Box 812, Yaoundé, Cameroon

³University of Maryland, A. James Clark School of Engineering, Department of Electrical and Computer Engineering, and Institute for Research in Electronics and Applied Physics (IREAP), 8279 Paint Branch Drive, College Park, Maryland 20742, USA

 (Received 22 July 2020; revised 17 September 2020; accepted 8 October 2020; published 23 October 2020)

We investigate the nonlinear dynamics of a recent architecture of an optoelectronic oscillator, where the emitting laser and the receiving diode are connected in a head-to-tail configuration via an optical fiber delay line. The resulting nonlinear transfer function is a piecewise linear profile, and its interplay with the delay leads to many complex behaviors such as relaxation oscillations and deterministic chaos. This system belongs to a recent class of optoelectronic oscillators where the nonlinearity does not originate from the sinusoidal transfer function of an imbalanced interferometer, and, in particular, it is a simple optoelectronic oscillator configuration that is capable of displaying a chaotic behavior. The results of the analytic study are confirmed by numerical simulations and experimental measurements.

DOI: [10.1103/PhysRevE.102.042217](https://doi.org/10.1103/PhysRevE.102.042217)

I. INTRODUCTION

Optoelectronic oscillators (OEOs) are nonlinear dynamical systems characterized by a feedback loop that associates an optical and an electrical branch [1,2]. These systems are generally delayed, as the signal round-trip delay time is not negligible with regards to the other timescales of the system. The scientific and technological interest in these systems arises from the fact that OEOs natively interconnect signals in the optical and radio-frequency ranges. This key property opened the way for applications in microwave generation [3–12], optical chaos cryptography [13–15], photonic neuromorphic computing [16–20], and sensing (see review article [21]).

The complex dynamics of OEOs has also been the focus of a large amount to fundamental research activities, driven by the necessity to understand in depth the nonlinear phenomena in these systems [22–33]. Indeed, the complex dynamics in OEOs mainly originates from the time delay, which is known to drastically expand the dimensionality of the system to infinity [34]. However, the exact nature of the nonlinear transfer function in the feedback loop also plays a major role in the complex dynamics of OEOs systems, because of sinusoidal transfer functions from imbalanced interferometers, such as phase or intensity electro-optic modulators. Alternative approaches use instead the laser itself as a nonlinear electrical-to-optical signal converter [35,36].

The dynamics of a semiconductor laser with AC-coupled nonlinear optoelectronic feedback has been experimentally

studied [37]. A period doubling sequence of small periodic and chaotic attractors is observed. The chaotic pulsing and the route to chaos in a semiconductor laser with delayed, positive optoelectronic feedback have been investigated numerically and experimentally [38]. In a laser with delayed feedback operating in an oscillatory regime, phase defects appear for delays longer than the oscillation period [39]. A nonlinear system with delayed feedback, whenever the delay time is much longer than the intrinsic correlation time, displays two widely separated timescales [40]. Experimental and theoretical researches, shows the existence of slow chaotic spiking sequences in the dynamics of a semiconductor laser with AC-coupled optoelectronic feedback [41].

The approach we are proposing is to use the effective “elbow” nonlinearity of the power-intensity (PI) transfer function of the emitting laser, which is a piecewise linear nonlinearity [42]. At the receiver end of the optical fiber delay line, the photodiode can also feature a nonlinearity of opposite nature, which is induced by saturation. The overall transfer function therefore cascades the laser and diode nonlinearities, and the goal of the present work is to show that, as a result, the OEO can be driven to fully developed chaos via a sequence of bifurcations when the gain is continuously increased. The advantage of studying this class of OEOs is essentially threefold. First, it permits one to build optoelectronic oscillators with a minimum amount of components, and, in particular, without electro-optic modulators. Such a modulator-less configuration is simpler to implement, and, since the lasers and photodiodes are the most affordable elements in the oscillator loop, it facilitates and simplifies overall the experimental study. Second, semiconductor lasers and photodiodes are easy to integrate at chip scale on the same platform, so that the architectures

*geraud.goune@yahoo.fr

we are exploring have the key advantage of being compatible with full integration. This integration process becomes significantly more complex if an electro-optical modulator has to be integrated as well. Finally, oscillators having piecewise linearity are ideal test benches to investigate nonlinear dynamics analytically. Piecewise linearity is for example the key property that has permitted the gain of significant theoretical understanding of the nonlinear dynamics of the Chua circuit, which has become a paradigmatic, widely studied chaotic system [43–45]. The effect of delayed time feedback in piecewise linear oscillators is also a topic that has investigated in recent years [46–48].

The plan of the article is the following. In the next section, we present the system under study along with the model used to investigate its complex dynamics. We perform the stability analysis of the system in Sec. III, while the numerical and experimental results are presented in Sec. IV A. The last section will conclude the article.

II. SYSTEM AND MODEL

The architecture of our OEO is displayed in Fig. 1, and it consists of five elements. The first one is the continuous-wave (CW) distributed feedback laser diode (LD) source operating at the telecom wavelength $\lambda = 1550$ nm. It has a threshold current $I_{th} = 16$ mA, and it is driven by a pump current $I_{pol} + I_{RF}(t)$, where I_{pol} is the polarization current, while $I_{RF}(t)$ is the time-varying radio-frequency (RF) current. The output of this laser diode has an output power $P(t)$ typically varying from 0 to 10 mW. The optical fiber delay line has a length $L = 40$ m, corresponding to a delay time $T = n_g L/c = 0.2$ μ s, where $n_g = 1.5$ is the group refraction index of the fiber and c is the velocity of light in vacuum. The optical signal is transduced into a photocurrent by an InGaAs photodiode (PD) with power-dependent responsivity $S(P)$, where S is a nonlinear function featuring a saturation profile. This photodiode has a 100 MHz bandwidth, and converts the input power $P(t)$ into an electric voltage $V(t)$ that is attenuated using a voltage variable attenuator (VVA), with the control voltage V_{cr} directly linked to the gain $G < 1$ and broadband bandwidth of

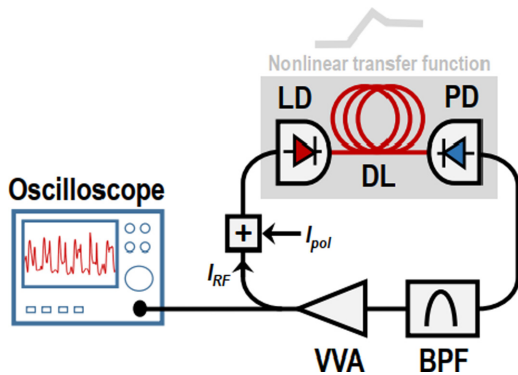


FIG. 1. Experimental setup of our OEO. The nonlinearity of the feedback loop is a piecewise linear transfer function. LD: Laser diode. DL: Delay line (optical fiber). PD: Photodiode. BPF: Bandpass filter. VVA: Variable voltage attenuator. I_{pol} : Polarization current. I_{RF} : Radio-frequency current.

0.01–2.5 GHz. This voltage is converted back into a current $I_{RF}(t)$, which is added to a polarization current I_{pol} using a bias tee (with bandwidth 0.1 MHz to 2.2 GHz) before being used to pump the laser diode, thereby closing the feedback loop.

The dynamical properties of the system are ruled by the overall bandpass filtering induced by the superimposed bandwidths of the RF amplifier, the photodiode, and the coupler. We can take advantage of the fact that the low and high cutoff frequencies $f_L = 530$ kHz and $f_H = 6.4$ MHz are distant one from each other in the spectral domain, and consider that this bandpass filter consists of two cascaded high-pass and low-pass first-order linear filters.

The input voltage $V_{in}(t)$ and output voltage $V_{out}(t)$ of the cascaded bandpass filter are linked by the equation

$$\left[1 + \frac{f_L}{f_H}\right] V_{out}(t) + \frac{1}{2\pi f_H} \frac{dV_{out}(t)}{dt} + 2\pi f_L \int_{t_0}^t V_{out}(s) ds = V_{in}(t). \quad (1)$$

The optical power P at the output of the optical fiber is converted into the electrical signal through the photodiode, according to the nonlinear relation $S \times P(t - T)$, where T is the time delay originating from the fiber propagation; this photodiode output voltage is in fact equal to the voltage $V_{in}(t)$ at the input of the bandpass filter. The relationship between $V_{RF}(t)$ and the output voltage is $V_{RF}(t) = \kappa G V_{out}(t)$. This voltage is converted into the current $I_{RF}(t) = V_{RF}(t)/R_Z$, where $R_Z = 50$ Ω is characteristic impedance used for the current-to-voltage conversion, while κ is a dimensionless factor standing for all the linear losses (electrical and optical) in the feedback loop.

It can therefore be shown that the radio-frequency voltage $V_{RF}(t)$ obeys the following equation:

$$\left[1 + \frac{f_L}{f_H}\right] V_{RF}(t) + \frac{1}{2\pi f_H} \frac{dV_{RF}(t)}{dt} + 2\pi f_L \int_{t_0}^t V_{RF}(s) ds = \frac{\kappa G}{R_Z} F[V_{RF}(t - T)] \quad (2)$$

where $F[V_{RF}(t - T)] = S \times P(t - T)$ is the piecewise linear transfer function of the feedback loop, which directly depends on the radio-frequency voltage.

If we take $f_L \ll f_H$ into account, Eq. (2) can be rewritten in the following dimensionless form:

$$x(t) + \tau \frac{dx(t)}{dt} + \frac{1}{\theta} \int_{t_0}^t x(s) ds = \beta F[x_T], \quad (3)$$

where the variable of the system is $x(t) = V_{RF}(t)/V_{REF}$, with $V_{REF} \equiv 1$ V being a convenient reference voltage for yielding $|x(t)| = |V_{RF}(t)|$. The delayed variable in this equation is $x_T \equiv x(t - T)$. The bandpass filter parameters of Eq. (3) are the timescales $\tau = 1/2\pi f_H = 25$ ns and $\theta = 1/2\pi f_L = 0.3$ μ s, and the dimensionless feedback loop gain $\beta = \frac{\kappa G}{R_Z}$.

To obtain our transfer function, we proceed with the experimental setup, which essentially consists of the laser diode and the photodiode. An input voltage is injected to the laser diode, we slowly increase it, and we record this voltage and the output voltage at the photodiode. The recorded data are used to plot the points obtained in Fig. 2. Finally we interpolate these points with a piecewise linear transfer function of the

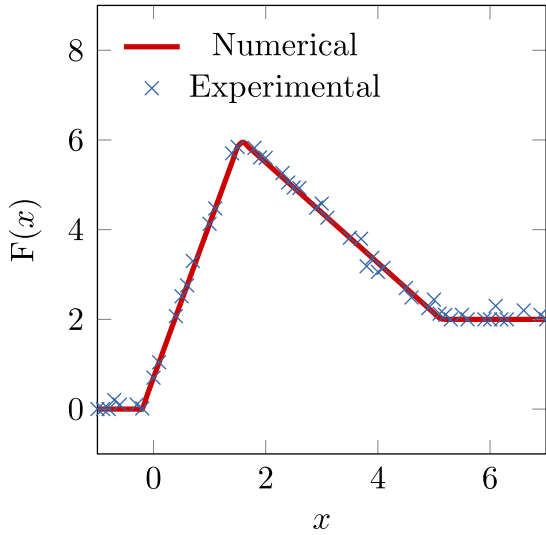


FIG. 2. Experimental and numerical transfer functions of the feedback loop. The polarization voltage of the semiconductor laser is adiabatically increased and output voltage of the photodiode is measured in the open-loop configuration. The numerical part is the plot of the piecewise linear function $F(x)$ given by Eq. (5).

form

$$F(x) = \begin{cases} a_1x + b_1 & \text{for } x \leq \alpha_1, \\ a_2x + b_2 & \text{for } \alpha_1 < x \leq \alpha_2, \\ a_3x + b_3 & \text{for } \alpha_2 < x \leq \alpha_3, \\ a_4x + b_4 & \text{for } x > \alpha_3. \end{cases} \quad (4)$$

The coefficients of the piecewise linear transfer function are determined with the linear interpolation between two known points. After solving Eq. (4), we obtain $a_1 = 0, b_1 = 0, a_2 = 3.43, b_2 = 0.70, a_3 = -1.12, b_3 = 7.74, a_4 = 0, b_4 = 2.00, \alpha_1 = -0.20, \alpha_2 = 1.55, \text{ and } \alpha_3 = 5.11$.

The dimensionless piecewise linear transfer function $F(x)$ is expressly defined as

$$F(x) = \begin{cases} 0 & \text{for } x \leq \alpha_1, \\ 3.43x + 0.70 & \text{for } \alpha_1 < x \leq \alpha_2, \\ -1.12x + 7.74 & \text{for } \alpha_2 < x \leq \alpha_3, \\ 2.00 & \text{for } x > \alpha_3. \end{cases} \quad (5)$$

The numerical Equation 5 is plotted in Fig. 2. The figure shows the good agreement between the experimental results and the numerical modeling.

Equation (3) is a nonlinear integrodifferential delay equation (IDDE), which can be conveniently rewritten in the form

$$\dot{y} = x, \quad (6)$$

$$\tau \dot{x} = -x - \frac{1}{\theta}y + \beta F[x_T], \quad (7)$$

where the overdot denotes the derivative with respect to time, $x_T \equiv x(t - T)$, and $y = \int_{t_0}^t x(s) ds$.

III. FIXED POINTS AND LINEAR STABILITY

The linear stability analysis is based on analyzing the time-dependent trajectory of the system when it is slightly perturbed from the steady state (x_0, y_0) . This fixed point has

to be perturbed as $(x, y) = (x + \delta x, y + \delta y)$, and we have to determine the asymptotic behavior of the perturbations. The perturbations can be considered dependent on the eigenvalue λ following $\delta x(\tau) \propto e^{\lambda\tau}$ and $\delta y(\tau) \propto e^{\lambda\tau}$. We examine the stability nature of the fixed points for Eqs. (6) and (7) both in the absence and in the presence of the time delay T .

A. Time delay $T = 0$

In the absence of time delay, the following fixed points can exist depending on the choice of parameters α_1, α_2 and α_3 in Eqs. (6) and (7).

(1) For $x \leq \alpha_1$, the fixed point is $(x_0, y_0) = (0, 0)$ and the characteristic equation in this region is

$$\tau\lambda^2 + \lambda + \frac{1}{\theta} = 0. \quad (8)$$

The solutions of this eigenvalue equation are

$$\lambda_{\pm} = \frac{1}{2\tau} \left[-1 \pm \sqrt{1 - 4\frac{\tau}{\theta}} \right]. \quad (9)$$

The fixed point is stable, since the values of λ are negative ($\lambda_{\pm} < 0$).

(2) For $\alpha_1 < x \leq \alpha_2$, the fixed point is $(x_0, y_0) = (0, 0.7\theta\beta)$ and the characteristic equation in this region is

$$\tau\lambda^2 + (1 - 3.43\beta)\lambda + \frac{1}{\theta} = 0. \quad (10)$$

The solutions of this eigenvalue equation are

$$\lambda_{\pm} = \frac{1}{2\tau} \left[-(1 - 3.43\beta) \pm \sqrt{(1 - 3.43\beta)^2 - 4\frac{\tau}{\theta}} \right]. \quad (11)$$

Its clear that at the critical point, $\beta_0 = 1/3.43$, there is a Hopf bifurcation as long as the quantity within the square root $(1 - 3.43\beta)^2 - 4\frac{\tau}{\theta}$ is less than zero. When $(1 - 3.43\beta) > 0$, there is a stable focus at the origin and we can see that, as $(1 - 3.43\beta)$ is changed from positive values to negative ones, the focus at the origin changes from being stable to unstable. The critical frequency and gain values at the Hopf bifurcation are therefore

$$\beta_0 = 0.29, \quad \omega_0 \simeq \frac{1}{\sqrt{\theta\tau}}. \quad (12)$$

(3) For $\alpha_2 < x \leq \alpha_3$, the fixed point is $(x_0, y_0) = (0, 7.74\theta\beta)$ and the characteristic equation in this region is

$$\tau\lambda^2 + (1 + 1.12\beta)\lambda + \frac{1}{\theta} = 0. \quad (13)$$

The solutions of this eigenvalue equation are

$$\lambda_{\pm} = \frac{1}{2\tau} \left[-(1 + 1.12\beta) \pm \sqrt{(1 + 1.12\beta)^2 - 4\frac{\tau}{\theta}} \right]. \quad (14)$$

The fixed point can only be stable, given the fact that $(1 + 1.12\beta) > 0$.

(4) For $x > \alpha_3$, the fixed point is $(x_0, y_0) = (0, 2\theta\beta)$ and the characteristic equation in this region is the same as that obtained in (i). Then the fixed point is stable.

Next we consider the case when time delay is present, $T > 0$.

B. Time delay $T > 0$

In the presence of time delay, we examine the stability as follows.

(1) For $x \leq \alpha_1$, the fixed point is $(x_0, y_0) = (0, 0)$, and the study of the stability remain the same as for the case $T = 0$: the fixed point is stable.

(2) For $\alpha_1 < x \leq \alpha_2$, the fixed point is $(x_0, y_0) = (0, 0.7\theta\beta)$ and the characteristic equation in this region is

$$\tau\lambda^2 + [1 - 3.43\beta e^{-\lambda T}]\lambda + \frac{1}{\theta} = 0, \quad (15)$$

The Hopf bifurcation occurs when $\lambda = i\omega$; it then follows from Eq. (15) that

$$\tau\omega^2 + 3.43\beta\omega \sin(\omega T) - \frac{1}{\theta} = 0, \quad (16)$$

$$3.43\beta \cos(\omega T) - 1 = 0, \quad (17)$$

which can be transformed into

$$\omega \tan(\omega T) = -\tau\omega^2 + \frac{1}{\theta}, \quad (18)$$

$$(3.43\beta)^2 = 1 + \left[\frac{1}{\theta\omega} - \tau\omega \right]^2, \quad (19)$$

when we assume $\tan(\omega_1 T) \simeq 0$. The trivial solution $\omega_1 T \simeq 2\pi$ is obtained and then introduced into Eq. (19) in order to obtain β_1 . The critical frequency and gain values at the Hopf bifurcation are therefore

$$\omega_1 \simeq \frac{2\pi}{T}, \quad \beta_1 \simeq \frac{1}{3.43} \left[1 + \left(\frac{T}{2\pi\theta} - \frac{2\pi\tau}{T} \right)^2 \right]^{\frac{1}{2}}. \quad (20)$$

Hence, from the above analysis, we anticipate that a first Hopf bifurcation will emerge close to $\beta_1 \simeq 0.35$, and lead to the emergence of a limit cycle of frequency $\omega_1 \simeq 2\pi \times 5$ MHz, which corresponds to T -periodic oscillations. when the regime changes, the frequency of oscillations becomes smaller, hence the approximation $\tan(\omega_2 T) \simeq \omega_2 T$. From solving Eqs. (18) and (19), we find that the critical frequency and gain corresponding to that second Hopf bifurcation are

$$\omega_2 \simeq \frac{1}{\sqrt{\theta(T+\tau)}}, \quad \beta_2 \simeq \frac{1}{3.43} \left[1 + \frac{(T+\tau)}{\theta} \right]^{\frac{1}{2}}. \quad (21)$$

Therefore, when β is increased and reaches the value $\beta_2 \simeq 0.38$, the limit cycle of frequency $\omega_2 \simeq 2\pi \times 612$ kHz emerges and becomes another stable attractor.

(3) For $\alpha_2 < x \leq \alpha_3$, the fixed point is $(x_0, y_0) = (0, 7.74\theta\beta)$ and the characteristic equation in this region is

$$\tau\lambda^2 + [1 + 1.12\beta e^{-\lambda T}]\lambda + \frac{1}{\theta} = 0. \quad (22)$$

The Hopf bifurcation occurs when $\lambda = i\omega$; then we solve it to obtain

$$\omega_3 \simeq \frac{2\pi}{T}, \quad \beta_3 \simeq \frac{1}{1.12} \left[1 + \left(\frac{T}{2\pi\theta} - \frac{2\pi\tau}{T} \right)^2 \right]^{\frac{1}{2}} \quad (23)$$

and

$$\omega_4 \simeq \frac{1}{\sqrt{\theta(T+\tau)}}, \quad \beta_4 \simeq \frac{1}{1.12} \left[1 + \frac{(T+\tau)}{\theta} \right]^{\frac{1}{2}}. \quad (24)$$

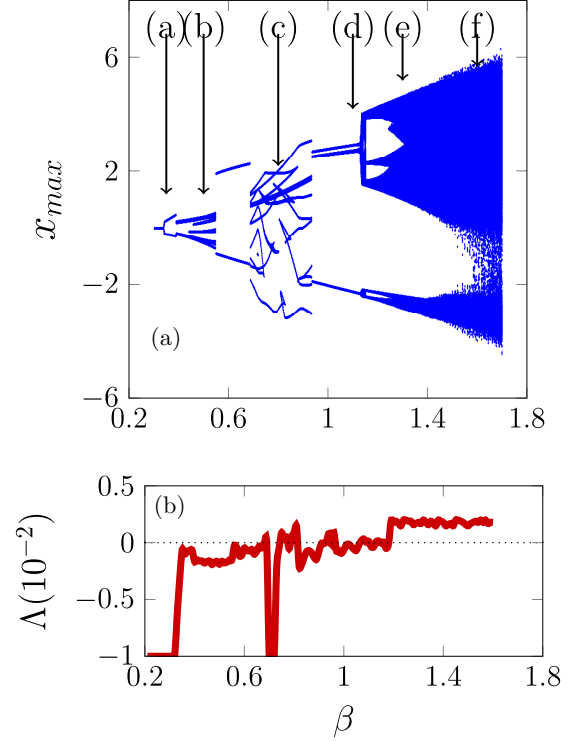


FIG. 3. (a) Numerical plots of the bifurcation diagram for the variable x (maxima). (b) Lyapunov exponent Λ of the system. The labels (a)–(f) indicate the dynamical regimes corresponding to the phase portraits of Fig. 4.

As the control parameter β is varied, the previous state loses its stability and two new branches of solutions emerge at the value $\beta_3 \simeq 1.08$ with the limit cycle of frequency $\omega_2 \simeq 2\pi \times 612$ kHz. These branches, in turn, lose their stability beyond a secondary bifurcation point $\beta_4 \simeq 1.17$, at the limit cycle of frequency $\omega_2 \simeq 2\pi \times 612$ kHz.

(4) For $x > \alpha_3$, the fixed point is $(x_0, y_0) = (0, 2\theta\beta)$ and the characteristic equation in this region is the same as that obtained in (i). Then the fixed point is stable.

IV. NUMERICAL AND EXPERIMENTAL RESULTS

A. Chaotic dynamic

The full bifurcation behavior of the system is displayed in the bifurcation diagram of Fig. 3(a). The bifurcation diagram is obtained by plotting the maxima of the variable $x(t)$ as a function of the control parameter β . In order to unambiguously quantify the occurrence of chaos, the main Lyapunov exponent of the system has been computed as

$$\Lambda = \lim_{t \rightarrow +\infty} \frac{1}{t} \ln \left[\frac{|\delta x(t)|}{|\delta x(t_0)|} \right], \quad (25)$$

where $|\delta x(t)|$ is the linear perturbation around the solution $x(t)$. It is known that a positive Lyapunov exponent is an indication of chaos, and the variations of Λ as a function of the gain β are displayed in Fig. 3(b). It can then be noted that in Fig. 3 both the bifurcation diagram and the Lyapunov exponent indicate the same window of chaotic behavior for the chosen parameters. A period doubling bifurcation sequence to

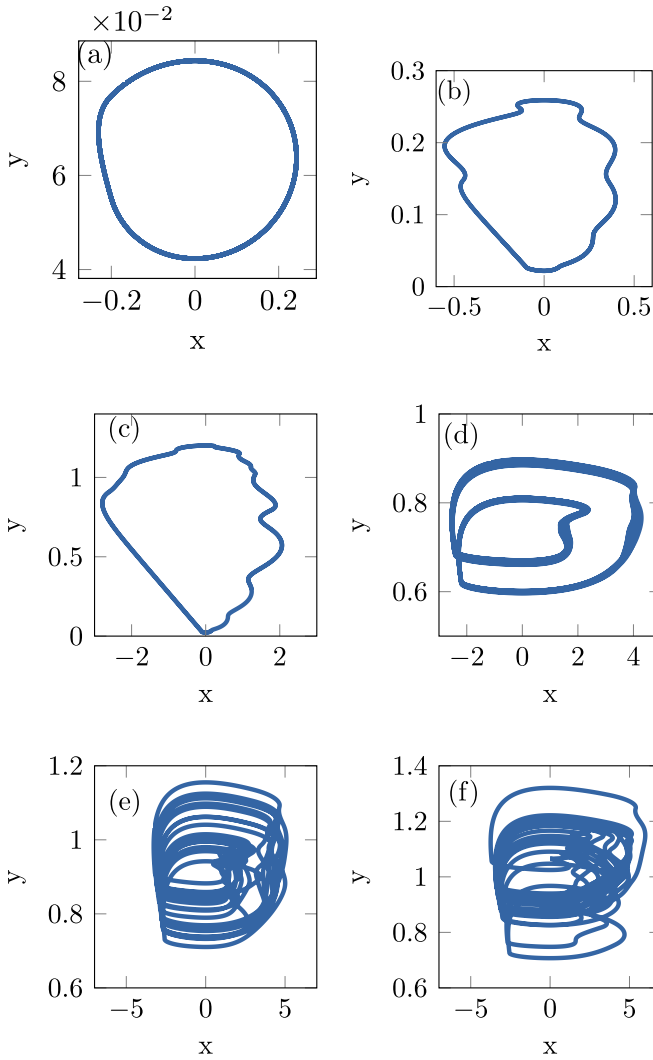


FIG. 4. Numerical simulations of Eqs. (6) and (7) for various gain values β in phase space. These phase portraits in the (x, y) plane correspond to the operating points highlighted in bifurcation diagram of Fig. 3(a): (a) period-limit cycle, $\beta = 0.35$, (b) $\beta = 0.5$, (c) $\beta = 0.8$, (d) $\beta = 1.2$, (e) $\beta = 1.5$, (f) chaotic attractor, $\beta = 1.7$.

chaos is observed for an initial range of β values. For instance, it is clear that for $0.35 < \beta < 0.38$ there is a limit-cycle attractor of period T . Many bifurcation changes in the dynamics take place at different critical values of β , particularly for $\beta > 0.38$, by a slow-scale limit cycle which appears when the feedback gain increased. We are interested in the complex regime of the system, when the control $\beta > 1.4$ the system exhibits a more complex chaotic motion as in Fig. 4(f).

B. Comparison between numerical and experimental results

Figure 5 shows an example of a complex wave-form signal when the bias parameter is tuned. In this figure we have displayed the experimental time traces along with the numerical ones obtained from the simulation of Eqs. (6) and (7). From the experimental viewpoint, the gain is varied through the control voltage V_{cr} of the VVA, while it is varied through β (which is proportional to G) for numerical simulations.

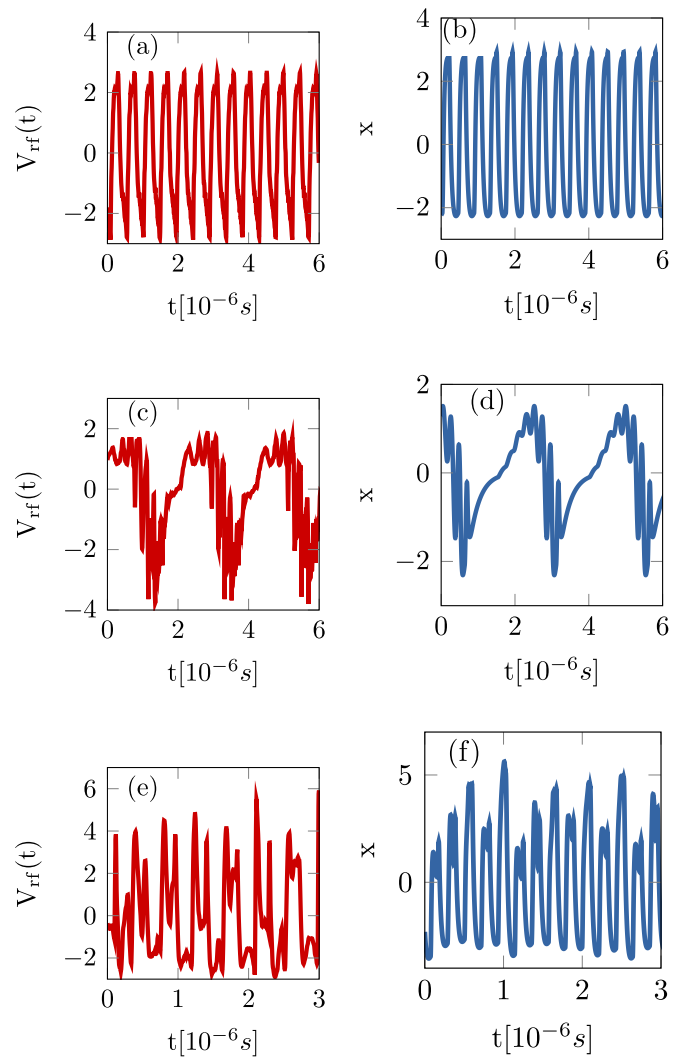


FIG. 5. Experimental (on the left) and numerical (on the right) time traces of the OEO. For the experimental results we set the polarization voltage at $V_{pol} = -2.5$ V, and the control voltage was set to (a) $V_{cr} = 26.6$ V, (c) $V_{cr} = 40$ V, (e) $V_{cr} = 45$ V. For the numerical simulations of Eqs. (7) and (6) we set $\tau = 25$ ns, $\theta = 0.3$ μ s, $T = 0.2$ μ s, and the feedback gain was set to (b) $\beta = 0.71$, (d) $\beta = 1.1$, (f) $\beta = 1.6$.

The polarization voltage is taken to allow the laser to reach the region of linear increase (note that, experimentally, the polarization voltages for the laser are negative in our setup). Figure 5(b) illustrates the fast T -periodic oscillations, which are observed for $\beta = 0.71$. This condition experimentally corresponds to $V_{cr} = 26.6$ V of Fig. 5(a). We slowly increased the control voltage, to obtain another wave-form signal. Figure 5(d) illustrates the slow-fast periodic oscillations, which are numerically observed for $\beta = 1.1$. This condition experimentally corresponds to $V_{cr} = 40$ V of Fig. 5(c). Figure 5(f) corresponds to the situation observed when β is further increased and has passed the bifurcation point $\beta = 1.6$. This signal typically indicates a state lacking order or predictability, that we call a chaotic signal. This condition experimentally corresponds to $V_{cr} = 45$ V of Fig. 5(e).

C. Discussion

When the delayed-feedback control parameter is included, we obtain a simple way to switch between stable and chaotic states. The good agreement between the experimental results and the numerical simulations validates the theoretical analysis. Optoelectronic feedback schemes have also found a lot of interest for the study of complex dynamics. They benefit from the possibility that the pump current of semiconductor lasers can be directly modulated with MHz or GHz bandwidths. In this simplest configuration, we have not used any modulator, such as a Mach-Zehnder modulator, and we have worked into the intermediate frequency range (10–100 MHz). The nonlinearity of the scheme is provided by the interactions of the nonlinear diode and the nonlinear photodetector. The system exhibit a rich variety of complex behavior, fast T -periodic oscillations with a frequency of $\omega_1 \simeq 2\pi \times 5$ MHz, slow-fast periodic oscillations with a frequency of $\omega_2 \simeq 2\pi \times 612$ kHz, and chaotic wave oscillations. The frequency in this slow-scale oscillation also depends in a nontrivial fashion on the three typical time constants of the system, namely τ , θ , and T . The critical values corresponding to these

Hopf bifurcations depend on these three time constants as well.

V. CONCLUSION

In conclusion, we have proposed a dynamical model for the study of nonlinear dynamics of the simplest laser-based optoelectronic oscillator with a nonlinear photodiode. The model shows that the interaction between the nonlinear transfer function of the laser diode and the time delay generates rich and complex dynamical regimes including fast-slow and chaotic oscillations that can be controlled by the feedback gain β . Finally, we expect this oscillator to be an interesting alternative for many other potential applications, including the synchronization and control of chaos. This OEO provides attractive and controllable dynamical features, of interest not only in chaos encryption, but also in real time and fast optical processing systems, such as random number generation, photonic ultrawideband signal generators, and reservoir computing taking advantage of the intrinsic multiple time scale of our OEO systems.

-
- [1] L. Maleki, *Nat. Photonics* **5**, 728 (2011).
- [2] L. Larger, *Proc. R. Soc. A* **371**, 20120464 (2013).
- [3] X. S. Yao and L. Maleki, *Electron. Lett.* **30**, 1525 (1994).
- [4] J. Yang, Y. Jin-Long, W. Yao-Tian, Z. Li-Tai, and Y. En-Ze, *IEEE Photonics Technol. Lett.* **19**, 807 (2007).
- [5] Y. K. Chembo, L. Larger, R. Bendoula, and P. Colet, *Opt. Express* **16**, 9067 (2008).
- [6] Y. K. Chembo, A. Hmima, P. A. Lacourt, L. Larger, and J. M. Dudley, *IEEE J. Lightwave Technol.* **27**, 5160 (2009).
- [7] I. Ozdur, M. Akbulut, N. Hoghooghi, D. Mandridis, M. U. Piracha, and P. J. Delfyett, *Opt. Lett.* **35**, 799 (2010).
- [8] O. Okusaga, E. J. Adles, E. C. Levy, W. Zhou, G. M. Carter, C. R. Menyuk, and M. Horowitz, *Opt. Express* **19**, 5839 (2011).
- [9] R. M. Nguimdo, Y. K. Chembo, P. Colet, and L. Larger, *IEEE J. Quantum Electron.* **48**, 1415 (2012).
- [10] S. Jia, J. Yu, J. Wang, W. Wang, Q. Wu, G. Huang, and E. Yang, *IEEE Photonics Technol. Lett.* **27**, 213 (2014).
- [11] K. Saleh, R. Henriet, S. Diallo, G. Lin, R. Martinenghi, I. V. Balakireva, P. Salzenstein, A. Coillet, and Y. K. Chembo, *Opt. Express* **22**, 32158 (2014).
- [12] Y. Zhang, D. Hou, and J. Zhao, *J. Lightwave Technol.* **32**, 2408 (2014).
- [13] A. Argyris, D. Syvridis, L. Larger, V. Annovazzi-Lodi, P. Colet, I. Fischer, J. Garcia-Ojalvo, C. R. Mirasso, L. Pesquera, and K. A. Shore, *Nature (London)* **438**, 343 (2005).
- [14] R. M. Nguimdo, R. Lavrov, P. Colet, M. Jacquot, Y. K. Chembo, and L. Larger, *J. Lightwave Technol.* **28**, 2688 (2010).
- [15] A. Uchida, *Optical Communication with Chaotic Lasers: Applications of Nonlinear Dynamics and Synchronization* (Wiley, New York, 2012).
- [16] L. Appeltant, M. C. Soriano, G. Van der Sande, J. Danckaert, S. Massar, J. Dambre, B. Schrauwen, C. R. Mirasso, and I. Fischer, *Nat. Commun.* **2**, 468 (2011).
- [17] Y. Paquot, F. Duport, A. Smerieri, J. Dambre, B. Schrauwen, M. Haelterman, and S. Massar, *Sci. Rep.* **2**, 287 (2012).
- [18] D. Brunner, M. C. Soriano, C. R. Mirasso, and I. Fischer, *Nat. Commun.* **4**, 1364 (2013).
- [19] F. Duport, A. Smerieri, A. Akrouf, M. Haelterman, and S. Massar, *Sci. Rep.* **6**, 22381 (2016).
- [20] L. Larger, A. Baylon-Fuentes, R. Martinenghi, V. S. Udaltsov, Y. K. Chembo, and M. Jacquot, *Phys. Rev. X* **7**, 011015 (2017).
- [21] X. Zou, X. Liu, W. Li, P. Li, W. Pan, L. Yan, and L. Shao, *IEEE J. Quantum Electron.* **52**, 0601116 (2016).
- [22] A. Neyer and E. Voges, *IEEE J. Quantum Electron.* **18**, 2009 (1982).
- [23] A. B. Cohen, B. Ravoori, T. E. Murphy, and R. Roy, *Phys. Rev. Lett.* **101**, 154102 (2008).
- [24] K. E. Callan, L. Illing, Z. Gao, D. J. Gauthier, and E. Scholl, *Phys. Rev. Lett.* **104**, 113901 (2010).
- [25] B. Ravoori, A. B. Cohen, J. Sun, A. E. Motter, T. E. Murphy, and R. Roy, *Phys. Rev. Lett.* **107**, 034102 (2011).
- [26] L. Weicker, T. Erneux, M. Jacquot, Y. Chembo, and L. Larger, *Phys. Rev. E* **85**, 026206 (2012).
- [27] L. Weicker, T. Erneux, O. D’Huys, J. Danckaert, M. Jacquot, Y. Chembo, and L. Larger, *Phys. Rev. E* **86**, 055201(R) (2012).
- [28] C. R. S. Williams, T. E. Murphy, R. Roy, F. Sorrentino, T. Dahms, and E. Schöll, *Phys. Rev. Lett.* **110**, 064104 (2013).
- [29] L. Weicker, T. Erneux, O. D’Huys, J. Danckaert, M. Jacquot, Y. K. Chembo, and L. Larger, *Philos. Trans. R. Soc. A* **371**, 20120459 (2013).
- [30] G. R. Goune Chengui, A. F. Talla, J. H. T. Mbe, A. Coillet, K. Saleh, L. Larger, P. Woafu, and Y. K. Chembo, *J. Opt. Soc. Am. B* **31**, 2310 (2014).
- [31] J. Martinez-Llinas, P. Colet, and T. Erneux, *Phys. Rev. E* **89**, 042908 (2014).
- [32] J. H. Talla Mbé, A. F. Talla, Geraud R. Goune Chengui, A. Coillet, L. Larger, P. Woafu, and Y. K. Chembo, *Phys. Rev. E* **91**, 012902 (2015).

- [33] A. M. Hagerstrom, T. E. Murphy, and R. Roy, *Proc. Natl. Acad. Sci. USA* **112**, 9258 (2015).
- [34] T. Erneux, *Applied Delay Differential Equations* (Springer, Berlin, 2010).
- [35] B. Romeira, J. Javaloyes, J. M. L. Figueiredo, C. N. Ironside, H. I. Cantu, and A. E. Kelly, *IEEE J. Quantum Electron.* **49**, 31 (2013).
- [36] B. Romeira, F. Kong, W. Li, J. M. L. Figueiredo, J. Javaloyes, and J. Yao, *IEEE J. Lightwave Technol.* **32**, 3933 (2014).
- [37] K. Al-Naimee, F. Marino, M. Ciszak, S. F. Abdalah, R. Meucci, and F. T. Arecchi, *Eur. Phys. J. D*, **58**, 187 (2010).
- [38] S. Tang and J. M. Liu, *IEEE J. Quantum Electron.* **37**, 329 (2001).
- [39] G. Giacomelli, R. Meucci, A. Politi, and F. T. Arecchi, *Phys. Rev. Lett.* **73**, 1099 (1994).
- [40] F. T. Arecchi, G. Giacomelli, A. Lapucci, and R. Meucci, *Phys. Rev. A* **45**, R4225(R) (1992).
- [41] K. Al-Naimee, F. Marino, M. Ciszak, R. Meucci, and F. Tito Arecchi, *New J. Phys.* **11**, 073022 (2009).
- [42] G. R. G. Chengui, P. Wofo, and Y. K. Chembo, *IEEE J. Lightwave Technol.* **34**, 873 (2016).
- [43] *Chua's Circuit: A Paradigm For Chaos*, edited by R. N. Madan (World Scientific, Singapore, 1993).
- [44] L. Fortuna, M. Frasca, and M. G. Xibilia, *Chua's Circuit Implementations: Yesterday, Today and Tomorrow* (World Scientific, Singapore, 2009).
- [45] R. Kilic, *A Practical Guide for Studying Chua's Circuits* (World Scientific, Singapore, 2010).
- [46] S. D. Cohen, D. Rontani, and D. J. Gauthier, *Chaos* **22**, 043112 (2012).
- [47] S. Tang, R. Vicente, M. C. Chiang, C. R. Mirasso, and J.-M. Liu, *IEEE J. Sel. Top. Quantum Electron.* **10**, 936 (2004).
- [48] M. C. Soriano, J. Garcia-Ojalvo, C. R. Mirasso, and I. Fischer, *Rev. Mod. Phys.* **85**, 421 (2013).